## A SYSTEM OF THREE SUPER EARTHS TRANSITING THE LATE K-DWARF GJ 9827 AT THIRTY PARSECS

Joseph E. Rodriguez<sup>1</sup>, Andrew Vanderburg<sup>2,1,\*</sup>, Jason D. Eastman<sup>1</sup>, Ian J. M. Crossfield<sup>3</sup>, David R. Ciardi<sup>4</sup>, David W. Latham<sup>1</sup>, Samuel N. Quinn<sup>1</sup>

<sup>1</sup>Harvard-Smithsonian Center for Astrophysics, 60 Garden St, Cambridge, MA 02138, USA
 <sup>2</sup>Department of Astronomy, The University of Texas at Austin, Austin, TX 78712, USA
 <sup>3</sup>Department of Physics, Massachusetts Institute of Technology, Cambridge, MA, USA
 <sup>4</sup>NASA Exoplanet Science Institute, California Institute of Technology, Pasadena, CA, USA and

 \*NASA Sagan Fellow

 Draft version December 14, 2024

#### **ABSTRACT**

We report the discovery of three small transiting planets orbiting GJ 9827, a bright (K = 7.2) nearby late K-type dwarf star. GJ 9827 hosts a  $1.64^{+0.22}_{-0.20}$   $R_{\oplus}$  super Earth on a 1.2 day period, a  $1.29^{+0.17}_{-0.16}$   $R_{\oplus}$  super Earth on a 3.6 day period, and a  $2.08^{+0.28}_{-0.26}$   $R_{\oplus}$  super Earth on a 6.2 day period. The radii of the planets transiting GJ 9827 span the transition between predominantly rocky and gaseous planets, and GJ 9827 b and c fall in or close to the known gap in the radius distribution of small planets between these populations. At a distance of  $\sim$ 30 parsecs, GJ 9827 is the closest exoplanet host discovered by K2 to date, making these planets well-suited for atmospheric studies with the upcoming *James Webb Space Telescope*. The GJ 9827 system provides a valuable opportunity to characterize interior structure and atmospheric properties of coeval planets spanning the rocky to gaseous transition.

Subject headings: planetary systems, planets and satellites: detection, stars: individual (GJ 9827)

#### 1. INTRODUCTION

With the confirmation of over 3500 planets to date and an additional  $\sim$ 4500 candidates from *Kepler*, the focus of studying exoplanets has largely shifted from pure discovery to understanding planetary demographics, system architectures, interior structures, and atmospheres. In particular, planets which transit their host stars are valuable for understanding the properties of small planets in detail. Like an eclipsing binary star, combining the transit light curve with radial velocity observations yields a measurement of the mass and radius of a planet relative to its star, which constrain the planet's interior structure. Planetary atmospheres can also be studied if the planet transits. The opacity of a planet's atmosphere depends on its chemical composition and the wavelength of the observation. This causes the apparent size of the planet to change as a function of wavelength. Therefore, by measuring the depth of the transit as a function of wavelength, it is possible to gain insight into the composition and temperature of the planet's atmosphere (this technique is known as transit transmission spectroscopy, Seager & Sasselov 2000; Brown 2001; Fortney et al. 2003).

Our ability to study the interior structures and atmospheres of planets, especially small planets ( $<4\,R_\oplus$ ) with small radial velocity and atmospheric signals, is highly dependent on the brightness of its host star. The brighter the host star, the easier it is to attain high enough signal-to-noise ratios to search for the small signals produced by small planets. The relative size of the planet to its host star is also highly important for transit transmission spectroscopy. It is easier to detect the small, wavelength-dependent changes in transit depth when planets are larger compared to their host stars, so small stars are more favorable targets than large stars for transit spectroscopy measurements. Therefore, nearby bright small stars with planets are excellent targets for atmospheric characterization (Burrows 2014).

Multi-planet systems provide the opportunity to compare

the atmospheres and interior structures of different planets while accounting for many confounding variables, like formation history and composition. In some cases, like the recently discovered seven-planet system transiting the nearby late M-dwarf TRAPPIST-1 (Gillon et al. 2016, 2017), it is possible to study similarly sized planets across orders of magnitude in incident flux. In terms of the stellar irradiation of the seven planets, TRAPPIST-1 c resembles Venus, TRAPPIST-1 d resembles the Earth, and TRAPPIST-1 f is similar to Mars (Gillon et al. 2017).

However, it would also be desirable to find a multi-planet system suitable for characterization which has planets with different sizes in order to understand the compositions of small planets ranging in size from similar to Earth to about four times the size of Earth. The Kepler mission has found a nearly ubiquitous population of planets with radii larger than the Earth but smaller than Neptune (Batalha et al. 2013; Howard et al. 2012; Petigura et al. 2013; Morton & Swift 2014; Christiansen et al. 2015; Dressing & Charbonneau 2015), for which we have no analogue in our own solar system. Recently, the California Kepler Survey (CKS) measured precise radii for over 2000 Kepler planets and found a bimodal distribution in the radii of small planets, with a deficit of planets with radii between 1.5 and 2.0  $R_{\oplus}$ , and two peaks in the radius distribution at about 1.3  $R_{\oplus}$  and 2.5  $R_{\oplus}$  (Fulton et al. 2017). The deficit in radii around 1.5-2  $R_{\oplus}$  is coincident with the transition (Weiss & Marcy 2014; Rogers 2015) between predominantly rocky planets (typically smaller than 1.6  $R_{\oplus}$ ) and planets with substantial gaseous envelopes (typically larger than 1.6  $R_{\oplus}$ ) as determined from mass measurements of a large number of sub-Neptune-sized planets discovered by Kepler (Wu & Lithwick 2013; Marcy et al. 2014; Hadden & Lithwick 2014, 2017). Since most of these planets with mass measurements orbit very close to their host stars (P<100 days), they receive a large amount of high-energy irradiation that can evaporate gaseous envelopes made of H/He

2 Rodriguez et al.

TABLE 1
GJ 9827 MAGNITUDES AND KINEMATICS

Other identifiers	HIP 115752 2MASS J23270480-0117108 EPIC 246389858			
Parameter	Description	Value	Source	
$\alpha_{J2000} \dots$	Right Ascension (RA)	23:27:04.83647	1	
$\delta_{J2000} \dots \dots$	Declination (Dec)	-01:17:10.5816	1	
$\mathbf{B}_T \dots \dots$	Tycho $B_T$ mag	$12.10 \pm 0.178$	2	
$V_T \dots \dots$	Tycho $V_T$ mag	$10.648 \pm 0.069$	2 3 3 3	
B	APASS Johnson B mag	$11.569 \pm 0.034$	3	
V	APASS Johnson V mag	$10.250 \pm 0.138$	3	
g'	APASS Sloan $g'$ mag	$10.995 \pm 0.021$	3	
r'	APASS Sloan $r'$ mag	9.845	3	
<i>i'</i>	APASS Sloan $i'$ mag	9.394	3	
J	2MASS <i>J</i> mag	$7.984 \pm 0.02$	4, 5	
Н	2MASS <i>H</i> mag	$7.379 \pm 0.04$	4, 5	
$K_S \dots \dots$	2MASS $K_S$ mag	$7.193 \pm 0.020$	4, 5	
WISE1	WISE1 mag	$6.990 \pm 0.041$	6	
WISE2	WISE2 mag	$7.155 \pm 0.02$	6	
WISE3	WISE3 mag	$7.114 \pm 0.017$	6	
<i>WISE4</i>	WISE4 mag	$6.957 \pm 0.107$	6	
$\mu_{\alpha}$	NOMAD proper motion . in RA (mas yr <sup>-1</sup> )	$374.4\pm2.2$	7	
$\mu_\delta$	NOMAD proper motion . in DEC (mas yr <sup>-1</sup> )	$215.7 \pm 1.9$	7	
$v \sin i_{\star} \dots$	Rotational velocity	$1.3\pm1.5~{\rm kms^{-1}}$	8	
[m/H]	Metallicity	$-0.5 \pm 0.1$	8	
$T_{ m eff}$	Effective Temperature	4270±100 K	8	
$\log(g)$	Surface Gravity	$4.9\pm0.2$ (cgs)	8	
$\pi$	Hipparcos Parallax (mas)	$32.98 \pm 1.76$	1	
d	Distance (pc)	$30.32 \pm 1.62$	1	
Spec. Type	Spectral Type	K6V	9	

NOTE. — References are: <sup>1</sup>van Leeuwen (2007), <sup>2</sup>Høg et al. (2000) <sup>3</sup>Henden et al. (2015), <sup>4</sup>Cutri et al. (2003), <sup>5</sup>Skrutskie et al. (2006), <sup>6</sup>Cutri & et al. (2014), <sup>7</sup>Zacharias et al. (2004), <sup>8</sup>Houdebine et al. (2016), <sup>9</sup>Stephenson (1986)

(Yelle 2004; Tian et al. 2005; Murray-Clay et al. 2009; Owen & Jackson 2012). The observed lack of planets with radii of 1.5-2.0  $R_{\oplus}$  could be due to these gaseous envelopes being evaporated away and leaving the smaller denser cores (Owen & Wu 2017).

In this paper, we present the discovery of three transiting planets orbiting the nearby (d=30.3  $\pm$  1.6 pc) star GJ 9827 using data from the K2 mission. The planets transiting GJ 9827 are the closest planets discovered by K2 (surpassing K2-18, at 34±4 pc Montet et al. 2015; Crossfield et al. 2016; Benneke et al. 2017). GJ 9827 b, c, and d are all super-Earth sized with radii  $R_b = 1.64^{+0.22}_{-0.20}~R_{\oplus}$ ,  $R_c = 1.29^{+0.17}_{-0.16}~R_{\oplus}$ ,  $R_d = 2.08^{+0.28}_{-0.26}~R_{\oplus}$ . Planets b  $(P_b = 1.209\text{d})$  and c  $(P_c = 3.648\text{d})$  orbit about half a percent outside of a 1:3 mean motion resonance, while planet d ( $P_d = 6.201$ ) orbits far from integer period ratios with the other two planets. The host is a bright (J $\approx$  8, H  $\approx$ 7.4,  $K \approx 7.2$ ) nearby late K star, making it an excellent target for atmospheric characterization with the upcoming James Webb Space Telescope (Gardner et al. 2006). The planets span the transition from rocky to gaseous planets, so the characteristics of their atmospheres and interior structures may illuminate how the structure and composition of small planets change with radius.

### 2. OBSERVATIONS AND ARCHIVAL DATA

# 2.1. K2 Photometry

In May 2013 the *Kepler* spacecraft experienced a failure of the second of its four reaction wheels, ending its primary mission. However, the Kepler spacecraft has been re-purposed to obtain high precision photometry for  $\sim$ 80 days at a time on a set of fields near the ecliptic in its extended K2 mission (Howell et al. 2014). During K2 Campaign 12, GJ 9827 was observed from UT 2016 December 16 until UT 2017 March 04. We identified GJ 9827 as a candidate planet host after downloading all of the *Kepler*-pipeline calibrated target pixel files from the Mikulski Archive for Space Telescopes, producing light curves, and correcting for K2 spacecraft systematics following Vanderburg & Johnson (2014) and Vanderburg et al. (2016b). We then searched the resulting light curves for transiting planet candidates using the pipeline described by Vanderburg et al. (2016b). Among the objects uncovered in our search were three super-Earth-sized planet candidates with periods of 1.2, 3.6, and 6.2 days around the nearby star GJ 9827. After we identified the signals, we re-processed the K2 light curve to simultaneously fit the transits, stellar variability, and K2 systematics. We flattened the light curve by dividing away the best-fit stellar variability (which we modeled as a basis spline with breakpoints every 0.75 days) from our simultaneous fit to the light curve. The final lightcurve has a noise level of 39 ppm per 30 minute cadence exposure, and a 6 hour photometric precision of 9 ppm. See Figure 1 for the final light curve.

The K2 light curve shows rotational stellar variability on GJ 9827 with a typical amplitude of about 0.2% peak to peak (See Figure 1). We calculated the autocorrelation function of the K2 light curve, and find a rotation period of  $31 \pm 1$  days, although it is possible the true rotation period is at about 16 days, or half our best estimate.

### 2.2. Archival Spectroscopy

As part of a survey of nearby Solar-type stars, GJ 9827 was observed on UT 2000 Aug 31 using the Center for Astrophysics (CfA) Digital Speedometer on the 1.5 m Wyeth Reflector at the Oak Ridge Observatory in the town of Harvard, Massachusetts. The Digital Speedometer measured an absolute RV of 31.2 km s<sup>-1</sup> with an approximate accuracy of  $\sim 0.3$  km s<sup>-1</sup>(Latham, private communication). GJ 9827 was also observed on UT 2010 Oct 08 and UT 2011 Aug 06 using a CORAVEL-type spectrometer at Vilnius University Observatory, which measured absolute RVs of GJ 9827 on these dates of 32.6 km s<sup>-1</sup> and 31.1 km s<sup>-1</sup>, respectively (Sperauskas et al. 2016). Using the equations given in Johnson & Soderblom (1987), the UVW space velocities of GJ 9827 were estimated to be (U,V,W) = (-59.2, 20.9, 30.6)km s<sup>-1</sup>(Sperauskas et al. 2016). From these observations, we see no evidence of any large RV variation over the span of over 10 years.

GJ 9827 was also observed twice in 2004 with the High Accuracy Radial Velocity Planet Searcher (HARPS) spectrograph as part of the guaranteed time collaboration's planet search, but not enough observations were taken to identify the small planet candidates we find. Later, Houdebine et al. (2016) used a principal component analysis based method to analyze the HARPS spectra and estimate stellar parameters. They found:  $T_{\rm eff} = 4270\pm100$ , [Fe/H]= -0.5 $\pm0.1$  dex,  $\log g = 4.9\pm0.2$ , and  $v\sin i_{\star} = 1.3\pm1.5$  km s<sup>-1</sup>. From the Hipparcos parallax and an analysis of the spectral energy distribution (SED), Houdebine et al. (2016) estimated the radius of

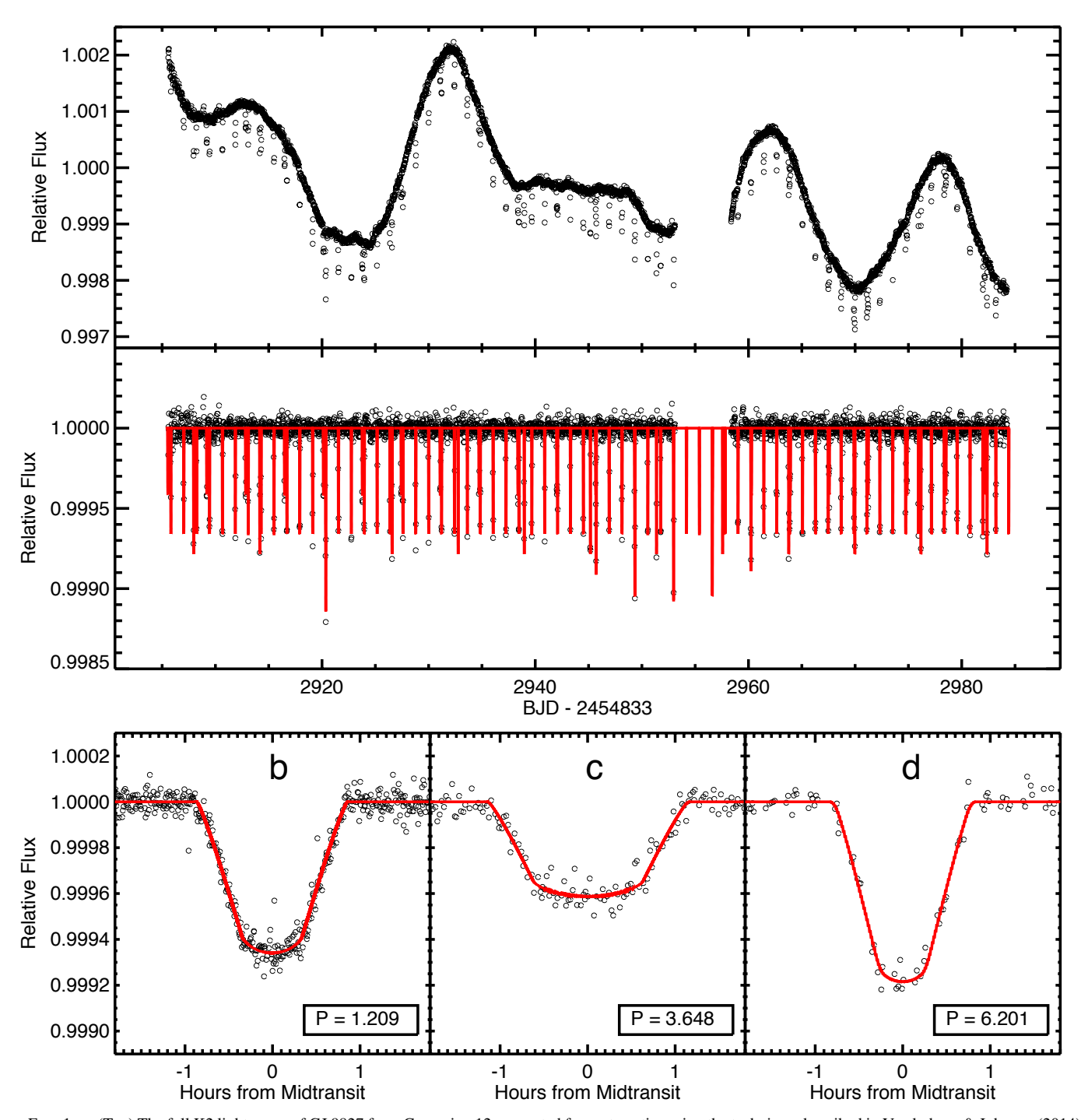


Fig. 1.— (Top) The full K2 light curve of GJ 9827 from Campaign 12, corrected for systematics using the technique described in Vanderburg & Johnson (2014) and Vanderburg et al. (2016b). (Middle) The corrected K2 lightcurve with best-fit low frequency variability removed. (Bottom) Phase folded K2 light curves of GJ 9827 b, c. and d. The observations are plotted in open black circles, and the best fit models are plotted in red.

GJ 9827 to be  $R_*$  of  $0.623\pm0.082~R_{\odot}$ . In this paper, we adopt the spectroscopic parameters and stellar radius from Houdebine et al. (2016).

# 2.3. Archival Seeing-Limited Imaging

Using archival observations from the National Geographic Society Palomar Observatory Sky Survey (NGS POSS) from 1953 and 1991 (ESO/SERC), we looked for nearby bright companions that may dilute our observed transit depths.

GJ 9827 has a high proper motion ( $\mu_{\alpha}$  = 374.4 mas and  $\mu_{\delta}$  = 215.7 mas), and has moved nearly 30" from its original position when the POSS image was taken in 1953 (See Figure 2). In 1953, GJ 9827 was outside of the region of sky enclosed within the photometric aperture we use to produce its modern K2 light curve. No background stars are present inside our K2 photometric aperture down to the POSS limiting magnitude of about R = 20, a full 10 magnitudes fainter than GJ 9827. Since all three transit signals around GJ 9827 have

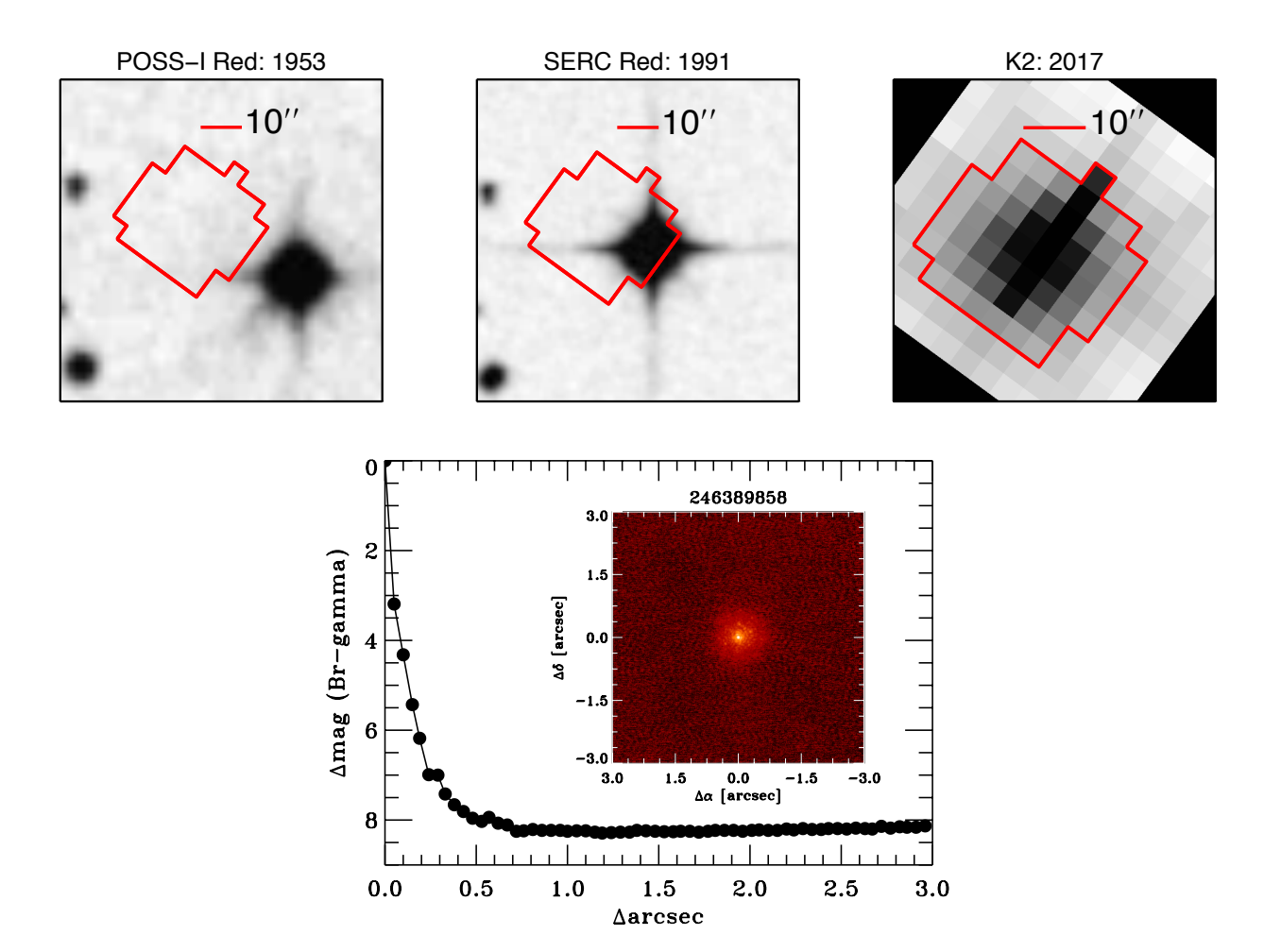


FIG. 2.— (Top Left) Archival imaging from the National Geographic Society Palomar Observatory Sky Survey (NGS POSS) of GJ 9827 taken with a red emulsion in 1953. (Top Middle) Archival imaging from the ESO/SERC survey of GJ 9827 taken with a red emulsion in 1991. (Top Right) Summed image of GJ 9827 from K2 observations. (Bottom) The Keck Br- $\gamma$  contrast curve and image (inset) of GJ 9827. We find no evidence of any additional components in the system.

depths greater than 100 ppm, the maximum depth of a transit caused by a background star 10 magnitudes fainter than GJ 9827, we can use "patient imaging" to confidently rule out background stars as the sources of these transit signals.

## 2.4. Keck/NIRC2 AO Imaging

Using the Near Infrared Camera 2 (NIRC2) behind the natural guide star adaptive optics system at the W. M. Keck Observatory, we obtained high resolution images of GJ 9827 using the Br- $\gamma$  filter on UT 2017 August 19. NIRC2 has a  $1024 \times 1024$  pixel array with a 9.942 mas pix<sup>-1</sup> pixel scale. The lower left quadrant of the NIRC2 array suffers from a higher noise level and a 3-point dither pattern was adopted excluding this regime of the detector. After flat-fielding and sky subtraction, each observation was shifted and co-added, resulting in the final image shown in Figure 2. No other star was detected in the 10'' field-of-view. To determine our sensitivity to companions, we inject simulated sources into the final image that have a signal to noise of 5. Figure 2 shows the  $5\sigma$  sensitivity as a function of spatial separation from GJ 9827, and the inset shows the image itself.

## 3. SYSTEM MODELING

Making use of the flattened K2 lightcurves, the Hipparcos parallax, and stellar parameters determined by Houdebine et al. (2016), we perform a global fit of the GJ 9827 system using EXOFASTv2 (Eastman et al. 2013, Eastman et. al., in prep). EXOFASTv2 is based heavily on EXO-FAST, but a large fraction of the code has been rewritten to be more flexible. EXOFASTv2 can now, among other things, simultaneously fit multiple planets, incorporate characterization observations (like Doppler Tomography), and simultaneously perform an SED within the global fit. EXOFASTv2 has a few major conceptual changes. First, an the error scaling term for the transit photometry is now fit within the Markov chain Monte Carlo (MCMC). Also, the fit uses the stepping parameters  $\log(M_*)$  and age instead of  $a/R_*$  and  $\log g$ . EX-OFASTv2 has previously been used to determine parameters for the HD 106315 system (Rodriguez et al. 2017).

Because GJ 9827 is relatively low-mass with marginal applicability to both the Torres relations (Torres et al. 2010) and YY isochrones (Yi et al. 2001), we disable those constraints within the global model, instead relying on just the  $R_*$  prior derived from Houdebine et al. (2016). The stellar mass,

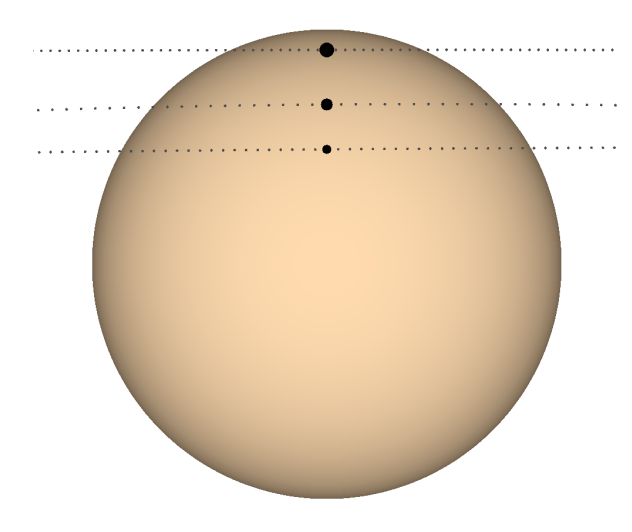


Fig. 3.— A diagram of the GJ 9827 system geometry shown with all planets at their respective transit centers. From top to bottom, the planets are d, b, and c. The color of the star matches its effective temperature, the planets are to scale with respect to each other and the host star, and the limb darkening matches our best-fit model in the Kepler band. The grey dots trace the orbital path of the planet, with a dot every three minutes. The curvature of planet b's orbit is plainly visible.  $\Omega$  for each planet (a rotation of the path about the center of the star) is assumed to be zero. Note the mutual inclinations may be much larger than implied here due to the ambiguity between the inclination and 180 degrees minus the inclination. Also note that the uncertainty in the impact parameters for planets b and c are large (see Figure 4).

then, is only constrained by the stellar density derived from the transit photometry and the prior on  $R_*$ . This stellar mass constraint is relatively weak, yielding  $M_* = 0.85^{+0.44}_{-0.30}~M_{\odot}$ . Therefore, we use the semi-empirical mass-absolute magnitude relation from (Mann et al. 2015) to independently derive a stellar mass of  $0.667\pm0.023~M_{\odot}$ . This value is consistent but far more precise than the value from our global fit. We adopt this mass for our discussion on characterizing the GJ 9827 system.

We performed a separate global fit using the broad band photometry summarized in Table 1, the Hipparcos parallax, an upper limit on extinction from Schlegel et al. (1998), to derive the radius of the star. This fit recovered a consistent stellar radius and uncertainty to Houdebine et al. (2016), but the stellar metalicity was driven too high, perhaps biased unfairly by the lack of SED models for such metal-poor stars.

From the Houdebine et al. (2016) analysis of HARPS South spectra combined with an SED analysis of GJ 9827, we set a prior on  $T_{\rm eff}$  of  $4270\pm100$  and  $R_*$  of  $0.623\pm0.082$   $R_\odot$ . Additionally, we imposed a prior on the parallax from Hipparcos (van Leeuwen 2007) and the limb-darkening parameters ( $u_1 = 0.44\pm0.1$  and  $u_2 = 0.26\pm0.1$ ) using the online Quadratic Limb Darkening applet from Eastman et al. (2016). While the limb darkening values can be derived within EXOFASTv2, we disabled it for this star out of an abundance of caution. Such a metal poor, low-mass star may suffer from systematic biases in the limb darkening and gaps in the parameter tables. While a small error in the limb darkening is well within the uncertainty of the K2 lightcurve, leav-

ing it enabled in the global fit may work backward to bias the  $\log g$ ,  $T_{\rm eff}$ , and [Fe/H] from which they are derived. The system parameters determined from our global fit are shown in Table 2 and a diagram of the system geometry is shown in Figure 3.

#### 4. STATISTICAL VALIDATION

To validate the planetary nature of the candidates identified to be transiting GJ 9827, we use the statistical techniques of Morton (2012) implemented in the vespa software package (Morton 2015). Using the location of the system in the sky and observational constraints, vespa calculates the false positive probability (FPP) of the transiting planet candidates. This takes into account the possibility of hierarchical companions or background objects that could lead to a false identification of a transiting planet. Since GJ 9827 hosts multiple planets it is very unlikely that all three planet candidates are false positives<sup>2</sup>. Previous works have calculated a "multiplicity boost" that reduces the false positive probability for multi-planet systems transiting a star in the original Kepler and K2 fields (Lissauer et al. 2012; Sinukoff et al. 2016; Vanderburg et al. 2016c). After applying the multiplicity boost to the vespa determined FPP for the planets transiting GJ 9827, we estimate a FPP of  $2 \times 10^{-6}$ ,  $6 \times 10^{-7}$ , and  $6 \times 10^{-10}$  for b, c, and d. Therefore, GJ 9827 b, c, and d are validated exoplanets.

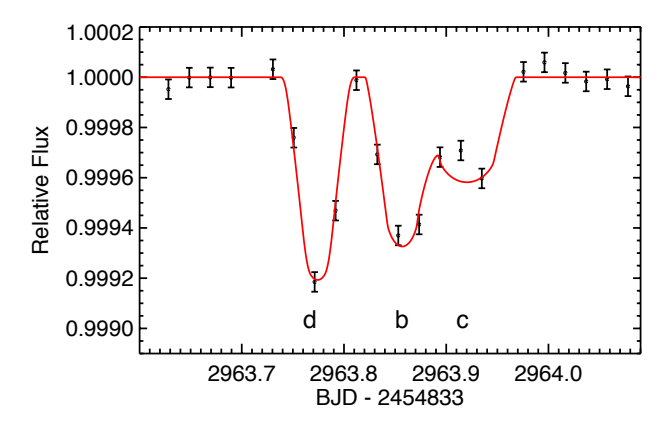
### 5. DISCUSSION

The proximity of GJ 9827 and its planetary architecture make it a compelling system worth further characterization. At  $\approx$ 30 parsecs, this is the closest exoplanet system discovered by K2 to date and one of the few stars to have multiple transiting terrestrial sized exoplanets that are well-suited for both mass measurements and atmospheric characterization. The host star is quite bright (V=10.3, J=8) and the measured planet radii of GJ 9827 b, c, and d are  $1.64^{+0.22}_{-0.20}$  $R_\oplus$ ,  $1.29^{+0.17}_{-0.16}$   $R_\oplus$ , and  $2.08^{+0.28}_{-0.26}$   $R_\oplus$ . As mentioned before, there is a known dichotomy in the sizes of short period (<100 days) small planets where planets are more commonly found to be less than  $1.5R_{\oplus}$  or larger than  $2.0R_{\oplus}$  (Fulton et al. 2017). Based on the mass measurements of planets in these two regimes, the larger planets are less dense and consistent with having a H/He envelope. It is thought that planets smaller than  $\sim 1.6~R_{\oplus}$  have lost this outer H/He envelope leaving the rocky core, explaining their higher densities and a lack of planets with radii of 1.5 to 2.0  $R_{\oplus}$  (Weiss & Marcy 2014; Rogers 2015). The three known planets orbiting GJ 9827 provide a rare opportunity to perform a comparative study since GJ 9827 c is  $<1.5R_{\oplus}$ , GJ 9827 d is  $>2.0R_{\oplus}$ , and GJ 9827 b lands right in this deficiency gap. This system may shed light on the evolution of planets within this radius regime.

Using the Weiss & Marcy (2014) mass-radius relations, we estimate the mass of GJ 9827 b, c, and d to be  $4.26^{+0.54}_{-0.49}~M_{\oplus}$ ,  $2.63^{+1.59}_{-1.00}~M_{\oplus}$ , and  $5.32^{+0.68}_{-0.62}~M_{\oplus}$ . Within our global model, EXOFASTv2 estimated the masses using the Chen & Kipping (2017) mass-radius relations to be  $3.52^{+1.4}_{-0.93}~M_{\oplus}$ ,  $2.46^{+0.89}_{-0.75}$ 

<sup>&</sup>lt;sup>1</sup> http://astroutils.astronomy.ohio-state.edu/exofast/limbdark.shtml

<sup>&</sup>lt;sup>2</sup> However, the chance that one of them is a false positive is harder to rule out (Latham et al. 2011).



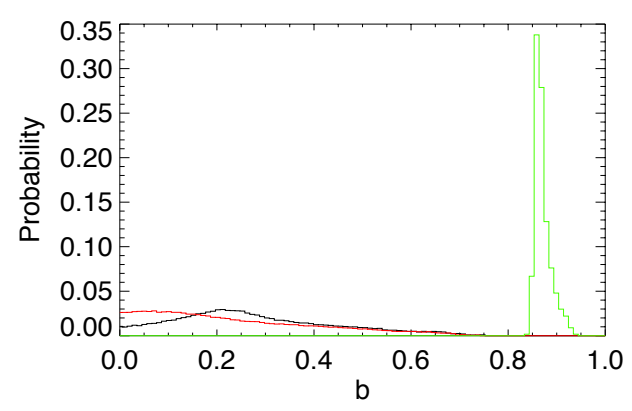


FIG. 4.— (Left) The corrected K2 lightcurve for GJ 9827 showing a simultaneous transit of b and c with the EXOFASTv2 model shown in red. (Right) The probability distribution of the impact parameter for GJ 9827 b (black), c (red), and d (green). We cannot rule out the possibility of mutual transits of GJ 9827 b and c

 $M_{\oplus}$ , and  $5.2^{+2.1}_{-1.5}$   $M_{\oplus}$ . We note that the Weiss & Marcy (2014) planet mass uncertainties ignore any uncertainty in the mass-radius relation itself, and is only due to the uncertainty in the radius. The Chen & Kipping (2017) estimated masses correspond to RV semi-amplitudes of  $2.34^{+0.90}_{-0.54}$  m s<sup>-1</sup>,  $1.08^{+0.44}_{-0.25}$  m s<sup>-1</sup>, and  $2.01^{+0.79}_{-0.48}$  m s<sup>-1</sup>. Houdebine et al. (2016) measured the rotational velocity of GJ 9827 to be <2 km s<sup>-1</sup>, making the planets around GJ 9827 well-suited for precise RV observations with current spectroscopic facilities to measure their masses. The rotation period of GJ 9827 is either 31d or 16d, well separated from the orbital periods of the planets, so it should be possible to filter away signals from stellar activity using techniques like Gaussian process regression (Haywood et al. 2014).

To better understand the feasibility of characterizing the atmospheres of the three planets orbiting GJ 9827, we calculate the atmospheric scale height and an expected signal-tonoise per transit following the description given in Vanderburg et al. (2016c). We repeat this calculation for all known planets where  $R_p < 3R_{\oplus}$  using NASA's Exoplanet archive (Akeson et al. 2013). It is expected that both GJ 9827 b and d might have thick gaseous atmospheres (Weiss & Marcy 2014), while GJ 9827 d likely does not have a thick envelope. We find that GJ 9827 b and d are two of the best small  $(R_n)$  $< 3R_{\oplus}$ ) exoplanets for detailed atmospheric characterization (See Table 3)<sup>3</sup>. By studying their atmospheric compositions, we may better understand the observed dichotomy in planetary composition observed at  $\sim 1.6~R_{\oplus}$ . All calculations are done using the H-band magnitude of the stars to test the feasibility of characterizing the planet's atmosphere with the *Hub*ble Space Telescope's Wide Field Camera 3 instrument and the upcoming suite of instruments that will be available on the James Webb Space Telescope. At a J-band magnitude of 8, GJ 9827 is near the expected saturation limit of the JWST instruments but should be accessible to all four instrument suites allowing for a high S/N with a relatively short exposure time: Near Infared Camera (NIRCam), Near Infrared Imager and Slitless Spectrograph (NIRISS), Near-Infrared Spectrograph (NIRSpec), and the Mid-Infrared Instrument (MIRI) (Beichman et al. 2014). The brightness of the GJ 9827 system makes it a great target for NIRCam's Dispersed Hartmann Sensor (DHS) mode (Schlawin et al. 2017).

The short orbital periods of the three GJ 9827 planets and the near 1 to 3 period commensurability between GJ 9827 b and c provides opportunities to observe overlapping transits of the three planets, as shown in Figure 4. The simultaneous transit on UT 2017 Feb 11 of GJ 9827 b and c shows one discrepant datapoint which misses the EXOFASTv2 model. This kind of discrepancy might be explained by a mutual transit, where GJ 9827 c actually transits both GJ 9827 and planet b simultaneously, which is not modeled by EXOFASTv2. However, at the observed time of this observation, the transit of planet b likely would have already completed (unless there was a significant transit timing variation). We do not find any convincing evidence of mutual transits in our analysis but based on the probability of each planet's impact parameters (See Figure 4), we are not able to rule out this possibility.

# 6. CONCLUSION

We present the discovery of three transiting planets orbiting the nearby late K-type star, GJ 9827. Two of the three planets are in near resonance orbits with periods of 1.2d and 3.6d, while the outer planet has a period of 6.2d. All three planets are super-Earth in size with radii of  $1.64^{+0.22}_{-0.20}~R_{\oplus}$ ,  $1.29^{+0.17}_{-0.16}~R_{\oplus}$ , and  $2.08^{+0.28}_{-0.26}~R_{\oplus}$ , for GJ 9827 b, c, and d, respectively. At only 30 pc from the Sun, this is the closest exoplanet system discovered by the K2 mission. The proximity and brightness of the host star combined with the similarity in the size of the three transiting planets make GJ 9827 an excellent target for comparative atmospheric characterization. The expected radial velocity semiamplitudes of the three planets are small but detectable with current instrumentation, especially given the star's fairly bright optical magnitude of V = 10.25. Radial velocity observations should be undertaken to measure the mass of each planet, to determine their interior structures for comparative studies. Mass measurements will also be critical for properly interpreting any atmospheric characterization through transit spectroscopy.

We thank Laura Kriedberg and Caroline Morley for their valuable conversations. Work performed by J.E.R. was sup-

<sup>&</sup>lt;sup>3</sup> We note that signal to noise is not everything. This calculation makes no assumptions about clouds or the presence of high-mean molecular weight atmospheres. The potential pitfalls of making these assumptions are illustrated by GJ 1214, which according to our calculation is the most amenable small planet to atmospheric characterization, but which shows no atmospheric features, likely due to the presence of clouds, hazes, or aerosols (Kreidberg et al. 2014).

 $TABLE\ 2 \\ Median\ values\ and\ 68\%\ confidence\ interval\ for\ GJ\ 9827.$ 

Parameter	Units		Values	_		
Stellar Parameters						
$M_*^{\dagger}\dots$	Mass from Relations $(M_{\odot})$	$0.667 \pm 0.023$				
$M_* \dots$	Mass from transits $(M_{\odot})$	$0.85^{+0.44}_{-0.30}$				
$R_*$	Radius $(R_{\odot})$	$0.85_{-0.30}^{+0.082}$ $0.630_{-0.077}^{+0.082}$				
$L_* \dots$	Luminosity $(L_{\odot})$	$0.119^{+0.035}_{-0.029}$				
$ ho_*\dots$	Density (cgs)	5.15+0.46				
$\log g \dots$	Surface gravity (cgs)	$4.786^{+0.074}_{-0.11}$				
Planetary Par	ameters:	b	c	d		
P	Period (days)	1.2089819+0.0000087	3.648086+0.000063	$6.201472 \pm 0.000061$		
a	Semi-major axis (AU)	$0.0211^{+0.0031}_{-0.0030}$	$3.648086^{+0.000063}_{-0.000060} \ 0.0440^{+0.0065}_{-0.00060}$	0.0627+0.0092		
$R_P \dots$	Radius $(R_{\oplus})$	$1.64^{+0.22}_{-0.00}$	$1.29^{+0.17}_{-0.16}$	$2.08^{+0.28}_{-0.26}$		
i	Inclination (Degrees)	88.0 <sup>+1.1</sup>	89.27+0.51	87.722 <sup>+0.077</sup>		
$T_{\mathrm{eq}}$	Equilibrium temperature (K)	1119+48	774+33	$648^{+28}$		
$\langle F \rangle \dots$	Incident Flux $(10^9 \text{ erg s}^{-1} \text{ cm}^{-2})$	$0.356^{+0.065}_{-0.041}$	$0.0816^{+0.015}_{-0.0094}$	$0.0402^{+0.0074}_{-0.0046}$		
$T_C \dots$	Time of Transit (BJD <sub>TDB</sub> )	$2905.82582 \pm 0.00033$	2000 100/0+0.00067	$2907.96107 \pm 0.00043$		
$T_S \dots$	Time of eclipse (BJD <sub>TDB</sub> )	$2906.43031^{+0.00033}_{-0.00032}$	2011 02344+0.00065	$2911.06181 \pm 0.00041$		
$T_A \dots \dots$	Time of Ascending Node (BJD <sub>TDB</sub> ).	$2905.52357 \pm 0.00033$	2908.28738 <sup>+0.00070</sup> 2908.28738 <sup>+0.00069</sup>	$2906.41070 \pm 0.00045$		
$T_D \dots$	Time of Descending Node (BJD <sub>TDB</sub> )	2906.12806 <sup>+0.00033</sup> <sub>-0.00032</sub> 0.02383 <sup>+0.00045</sup> <sub>-0.00047</sub>	$2910.11142^{+0.00066}_{-0.00072}$	$2909.51144 \pm 0.00042$		
$R_P/R_*$ .	Radius of planet in stellar radii	$0.02383^{+0.000045}_{-0.00047}$	$0.01872^{+0.00038}_{-0.00033}$	$0.03017^{+0.00075}_{-0.00060}$		
$a/R_* \dots$	Semi-major axis in stellar radii	$7.35^{+0.22}_{-0.56}$	$15.35^{+0.45}_{-1.2}$	$21.87^{+0.64}_{-1.7}$		
$d/R_* \dots$	Separation at mid transit	$7.35^{+0.22}_{-0.56}$	$15.35^{-1.45}_{1.2}$	$21.87^{-0.64}_{-1.7}$		
$b \dots \dots$	Impact parameter	$0.26^{+0.20}_{-0.14}$	$0.20^{+0.24}_{-0.14}$	$0.8713^{+0.021}_{-0.0001}$		
$\delta \dots \dots$	Transit depth	$0.000568 \pm 0.000022$	$0.000350^{+0.000014}_{-0.000012}$	$0.000911^{+0.000046}_{-0.00036}$		
Depth	Flux decrement at mid transit	$0.000568 \pm 0.000022$	0.000350+0.000014	$0.000911^{+0.000036}_{-0.000036}$		
$P_T$	A priori non-grazing transit prob	$0.1328^{+0.011}_{-0.0038}$	$0.0639^{+0.00012}_{-0.0018}$	$0.0443^{+0.0037}_{-0.0012}$		
$P_{T,G}\dots$	A priori transit prob	$0.1392^{+0.012}_{+0.022}$	$0.0663^{+0.0055}_{-0.0010}$	$0.0471^{+0.0039}_{-0.0014}$		
$T_{\mathrm{FWHM}}$	FWHM duration (days)	$0.05054^{+0.0010}_{-0.0000}$	$0.0738^{+0.0012}_{-0.0014}$	$0.0439^{+0.0017}_{-0.0010}$		
au	Ingress/egress duration (days)	$0.001291^{+0.00027}_{-0.000070}$	$0.001432^{+0.00029}_{-0.00055}$	$0.00558^{+0.0011}_{-0.0037}$		
$T_{14} \ldots$	Total duration (days)	$0.05196^{+0.0010}_{-0.00086}$	$0.0754^{+0.0013}_{-0.0015}$	$0.0498^{+0.0015}_{-0.0012}$		
Wavelength Parameters:		Kepler				
<i>u</i> <sub>1</sub>	linear limb-darkening coeff	$0.402^{+0.078}_{-0.076}$				
$u_1 \dots u_2 \dots u_2 \dots$	quadratic limb-darkening coeff	$0.402_{-0.076} \\ 0.232 \pm 0.093$				
Transit Parameters:		Kepler				
$F_0 \dots F_0 \dots$	Added Variance	$ \begin{array}{c} -0.0000000000003^{+0.000000000037}_{-0.000000000036} \\ 0.99999997 \pm 0.000000070 \end{array}$				

NOTE. — NOTES: All timestamps are reported in BJD<sub>TDB</sub>-2454833

ported by the Harvard Future Faculty Leaders Postdoctoral fellowship. This work was performed in part under contract with the California Institute of Technology (Caltech)/Jet Propulsion Laboratory (JPL) funded by NASA through the Sagan Fellowship Program executed by the NASA Exoplanet Science Institute. This paper includes data collected by the *Kepler*/K2 mission. Funding for the *Kepler* mission is provided by the NASA Science Mission directorate. Some of the data presented in this paper were obtained from the Mikulski Archive for Space Telescopes (MAST). STScI is operated by the Association of Universities for Research in Astronomy,

Inc., under NASA contract NAS5–26555. Support for MAST for non–HST data is provided by the NASA Office of Space Science via grant NNX13AC07G and by other grants and contracts. Some of the data presented herein were obtained at the WM Keck Observatory (which is operated as a scientific partnership among Caltech, UC, and NASA). The authors wish to recognize and acknowledge the very significant cultural role and reverence that the summit of Mauna Kea has always had within the indigenous Hawaiian community. We are most fortunate to have the opportunity to conduct observations from this mountain.

### REFERENCES

Akeson, R. L., Chen, X., Ciardi, D., et al. 2013, PASP, 125, 989 Batalha, N. M., Rowe, J. F., Bryson, S. T., et al. 2013, ApJS, 204, 24 Beichman, C., Benneke, B., Knutson, H., et al. 2014, PASP, 126, 1134 Benneke, B., Werner, M., Petigura, E., et al. 2017, ApJ, 834, 187 Brown, T. M. 2001, ApJ, 553, 1006 Burrows, A. S. 2014, Nature, 513, 345

<sup>†</sup> Estimated mass of GJ9827 using the Mann et al. (2015) mass-radius relations. This value was not used in determining the transit or planetary parameters.

TABLE 3 The Best Confirmed Planets for Transmission Spectroscopy with  $R_P < 3\,R_\oplus$ 

Planet	$R_P(R_{\oplus})$	S/Na	Reference
GJ 1214 b	$2.85{\pm}0.20$	1.00	Charbonneau et al. (2009)
55 Cnc e <sup>b</sup>	$1.91 \pm 0.08$	0.41	Dawson & Fabrycky (2010)
HD 97658 b	$2.34^{+0.17}_{-0.15}$	0.36	Dragomir et al. (2013)
TRAPPIST-1f	$1.045\pm0.038$	0.24	(Gillon et al. 2017)
GJ 9827 b	$1.64^{+0.22}_{-0.20} R_{\oplus}$	0.14	this work
HD 3167 c	$2.85^{+0.24}_{-0.15}$	0.14	Vanderburg et al. (2016c); Christiansen et al. (2017)
HIP 41378 b	$2.90\pm0.44$	0.14	Vanderburg et al. (2016a)
GJ 9827 d	$2.08^{+0.28}_{-0.26} R_{\oplus}$	0.13	this work
K2-28 b	$2.32\pm0.24$	0.12	Hirano et al. (2016)
HD 106315 b	2.5±0.1	0.10	(Crossfield et al. 2017; Rodriguez et al. 2017)

NOTES: "The predicted signal-to-noise ratios relative to GJ 1214 b. All values used in determining the signal-to-noise were obtained from the NASA Exoplanet Archive (Akeson et al. 2013). If a system did not have a reported mass on NASA Exoplanet Archive or it was not a  $2\sigma$  result, we used the Weiss & Marcy (2014) Mass-Radius relationship to estimate the planet's mass. <sup>b</sup>Our calculation for the S/N of 55 Cnc e assumes a H/He envelope since it falls just above the pure rock line determined by Zeng et al. (2016). However, 55 Cnc e is in a ultra short period orbit, making it unlikely that it would hold onto a thick H/He envelope.

Charbonneau, D., Berta, Z. K., Irwin, J., et al. 2009, Nature, 462, 891 Chen, J., & Kipping, D. 2017, ApJ, 834, 17

Christiansen, J. L., Clarke, B. D., Burke, C. J., et al. 2015, ApJ, 810, 95 Christiansen, J. L., Vanderburg, A., Burt, J., et al. 2017, ArXiv e-prints, arXiv:1706.01892

Crossfield, I. J. M., Ciardi, D. R., Petigura, E. A., et al. 2016, ApJS, 226, 7 Crossfield, I. J. M., Ciardi, D. R., Isaacson, H., et al. 2017, ArXiv e-prints, arXiv:1701.03811

Cutri, R. M., & et al. 2014, VizieR Online Data Catalog, 2328, 0

Cutri, R. M., Skrutskie, M. F., van Dyk, S., et al. 2003, VizieR Online Data Catalog, 2246, 0

Dawson, R. I., & Fabrycky, D. C. 2010, ApJ, 722, 937

Dragomir, D., Matthews, J. M., Eastman, J. D., et al. 2013, ApJ, 772, L2 Dressing, C. D., & Charbonneau, D. 2015, ApJ, 807, 45

Eastman, J., Gaudi, B. S., & Agol, E. 2013, PASP, 125, 83

Eastman, J. D., Beatty, T. G., Siverd, R. J., et al. 2016, AJ, 151, 45

Fortney, J. J., Sudarsky, D., Hubeny, I., et al. 2003, ApJ, 589, 615 Fulton, B. J., Petigura, E. A., Howard, A. W., et al. 2017, ArXiv e-prints, arXiv:1703.10375

Gardner, J. P., Mather, J. C., Clampin, M., et al. 2006, Space Sci. Rev., 123,

Gillon, M., Jehin, E., Lederer, S. M., et al. 2016, Nature, 533, 221 Gillon, M., Triaud, A. H. M. J., Demory, B.-O., et al. 2017, Nature, 542, 456

Hadden, S., & Lithwick, Y. 2014, ApJ, 787, 80 . 2017, AJ, 154, 5

Haywood, R. D., Collier Cameron, A., Queloz, D., et al. 2014, MNRAS, 443, 2517

Henden, A. A., Levine, S., Terrell, D., & Welch, D. L. 2015, in American Astronomical Society Meeting Abstracts, Vol. 225, American Astronomical Society Meeting Abstracts, 336.16

Hirano, T., Fukui, A., Mann, A. W., et al. 2016, ApJ, 820, 41 Høg, E., Fabricius, C., Makarov, V. V., et al. 2000, A&A, 355, L27

Houdebine, E. R., Mullan, D. J., Paletou, F., & Gebran, M. 2016, ApJ, 822,

Howard, A. W., Marcy, G. W., Bryson, S. T., et al. 2012, ApJS, 201, 15 Howell, S. B., Sobeck, C., Haas, M., et al. 2014, PASP, 126, 398 Johnson, D. R. H., & Soderblom, D. R. 1987, AJ, 93, 864 Kreidberg, L., Bean, J. L., Désert, J.-M., et al. 2014, Nature, 505, 69 Latham, D. W., Rowe, J. F., Quinn, S. N., et al. 2011, ApJ, 732, L24 Lissauer, J. J., Marcy, G. W., Rowe, J. F., et al. 2012, ApJ, 750, 112

Mann, A. W., Feiden, G. A., Gaidos, E., Boyajian, T., & von Braun, K. 2015, ApJ, 804, 64

Marcy, G. W., Isaacson, H., Howard, A. W., et al. 2014, ApJS, 210, 20 Montet, B. T., Morton, T. D., Foreman-Mackey, D., et al. 2015, ApJ, 809, 25 Morton, T. D. 2012, ApJ, 761, 6

. 2015, VESPA: False positive probabilities calculator, Astrophysics Source Code Library, ascl:1503.011

Morton, T. D., & Swift, J. 2014, ApJ, 791, 10

Murray-Clay, R. A., Chiang, E. I., & Murray, N. 2009, ApJ, 693, 23

Owen, J. E., & Jackson, A. P. 2012, MNRAS, 425, 2931

Owen, J. E., & Wu, Y. 2017, ArXiv e-prints, arXiv:1705.10810

Petigura, E. A., Howard, A. W., & Marcy, G. W. 2013, Proceedings of the National Academy of Science, 110, 19273

Rodriguez, J. E., Zhou, G., Vanderburg, A., et al. 2017, AJ, 153, 256 Rogers, L. A. 2015, ApJ, 801, 41

Schlawin, E., Rieke, M., Leisenring, J., et al. 2017, PASP, 129, 015001 Schlegel, D. J., Finkbeiner, D. P., & Davis, M. 1998, ApJ, 500, 525

Seager, S., & Sasselov, D. D. 2000, ApJ, 537, 916 Sinukoff, E., Howard, A. W., Petigura, E. A., et al. 2016, ApJ, 827, 78

Skrutskie, M. F., Cutri, R. M., Stiening, R., et al. 2006, AJ, 131, 1163 Sperauskas, J., Bartašiūtė, S., Boyle, R. P., et al. 2016, A&A, 596, A116 Stephenson, C. B. 1986, AJ, 92, 139

Tian, F., Toon, O. B., Pavlov, A. A., & De Sterck, H. 2005, ApJ, 621, 1049 Torres, G., Andersen, J., & Giménez, A. 2010, A&A Rev., 18, 67 van Leeuwen, F. 2007, A&A, 474, 653

Vanderburg, A., & Johnson, J. A. 2014, PASP, 126, 948

Vanderburg, A., Becker, J. C., Kristiansen, M. H., et al. 2016a, ApJ, 827, L10

Vanderburg, A., Latham, D. W., Buchhave, L. A., et al. 2016b, ApJS, 222, 14 Vanderburg, A., Bieryla, A., Duev, D. A., et al. 2016c, ApJ, 829, L9

Weiss, L. M., & Marcy, G. W. 2014, ApJ, 783, L6

Wu, Y., & Lithwick, Y. 2013, ApJ, 772, 74

Yelle, R. V. 2004, Icarus, 170, 167

Yi, S., Demarque, P., Kim, Y.-C., et al. 2001, ApJS, 136, 417

Zacharias, N., Monet, D. G., Levine, S. E., et al. 2004, in Bulletin of the American Astronomical Society, Vol. 36, American Astronomical Society Meeting Abstracts, 1418

Zeng, L., Sasselov, D. D., & Jacobsen, S. B. 2016, ApJ, 819, 127